UNIVERSITY of York

This is a repository copy of *All Current Sensors Survivable IPMSM Drive with Reconfigurable Inverter*.

White Rose Research Online URL for this paper:
https://eprints.whiterose.ac.uk/id/eprint/162735/

Version: Accepted Version

Article:
Lu, Jiadong, Hu, Yihua, Liu, Jinglin et al. (1 more author) (2020) All Current Sensors Survivable IPMSM Drive with Reconfigurable Inverter. IEEE Transactions on Industrial Electronics. pp. 6331-6341. ISSN: 0278-0046

https://doi.org/10.1109/TIE.2019.2937070

Reuse
Items deposited in White Rose Research Online are protected by copyright, with all rights reserved unless indicated otherwise. They may be downloaded and/or printed for private study, or other acts as permitted by national copyright laws. The publisher or other rights holders may allow further reproduction and re-use of the full text version. This is indicated by the licence information on the White Rose Research Online record for the item.

Takedown
If you consider content in White Rose Research Online to be in breach of UK law, please notify us by emailing eprints@whiterose.ac.uk including the URL of the record and the reason for the withdrawal request.

White Rose university consortium
Universities of Leeds, Sheffield & York

eprints@whiterose.ac.uk
https://eprints.whiterose.ac.uk/

All Current Sensors Survivable IPMSM Drive with Reconfigurable Inverter

Jiadong Lu, *Member, IEEE*, Yihua Hu, *Senior Member, IEEE,* Jinglin Liu, *Member, IEEE,* and Zheng Wang, *Senior Member, IEEE*

***Abstract*—The conventional phase current reconstruction strategies utilize a DC-bus current sensor to reproduce the three-phase currents during phase current sensor faults. However, no current sensor is guaranteed to be healthy in an actual drive. It means that the only survived current sensor may not be accidentally located at the DC-bus side, and it can also be at the phase side. In addition, previous studies focus on a particular inverter topology for current reconstruction, whose fault-tolerant capability is threatened when the inverter topology is changed due to malfunctions. This paper proposes a survivable IPMSM drive that realizes the current reconstruction purpose whichever the only survived current sensor is. Besides, inverter topology reconfiguration can be realized by not changing the wirings of the current sensors. Most important of all, the proposed strategy does not affect the normal operations of the drive when no fault occurs. The effectiveness of the proposed strategy is verified by experimental results on a 5kW IPMSM motor prototype, which shows that the reconstructed phase currents track the actual ones accurately in different failure conditions.**

***Index Terms*—Current reconstruction, interior permanent magnet synchronous motor (IPMSM), reconfigurable inverter, survivable drive.**

I. Introduction

OWING to its outstanding advantages, interior permanent magnet synchronous motor (IPMSM) shows excellent application prospects [1]-[3] compared to other motors [4]. An IPMSM drive usually contains several key components, i.e., an inverter and multiple current sensors. The faults of these key components will make the system out of service. To solve this thorny problem, many fault-tolerant control technologies are proposed [5]-[9]. For inverter with one bridge arm open-circuit fault, the three-phase four-switch (TPFS) topology is proposed [10]-[12]. To deal with the phase current sensor faults, the phase current reconstruction strategy is put forward [13]-[16].

Generally, an IPMSM drive has one DC-bus and three (two at least for the drives without neutral line) phase current sensors [17]. The current reconstruction strategy utilizes a single current sensor for recovery of the three-phase currents in case that the phase-current sensors malfunction [18]. Usually, the single current sensor applied in the current reconstruction strategies is the DC-bus current sensor [19]-[21]. Because the DC-bus current is related to the three-phase currents according to different switching states, it is possible to realize current reconstruction by a single DC-bus current sensor. The phase current reconstruction strategy is applied in a three-phase direct matrix converter drive system by using the space vector modulation control technique in [13]. The measurement vector insertion method is proposed in [14], in which the three inserted voltage vectors generate an equivalent zero vector that has minimum impacts on the machine's performance and operating envelope. In [18], the impact of the offset error of the DC-bus current sensor on the current reconstruction strategy is analyzed, where the compensation method is also raised. In addition, the overmodulation method for the single current sensor driven IPMSM system is studied in [19]. The current measurement errors are discussed in [22], where the impact of rotor speed on position information is taken into account. Considering sensor error detection and compensation, self-healing methods for the multiple sensors in a motor drive are studied in [23], [24]. Three independent observers are integrated in [24], which can detect and localize the faults and switch the system to tolerant vector control mode even only one healthy phase current sensor is available. In [25] and [26], the current measurement error introduced by the current sensor itself is analyzed in detail, where the offset and scaling errors are taken into consideration. No additional hardware but the commanded voltage reference of the current controller is required in the compensation method in [26]. As the current reconstruction strategy usually needs significant changes on the PWM synthesis method for the satisfaction of the minimum action time requirement, the traditional symmetrical seven segment SVPWM technology is difficult to be applied in these methods. To solve this problem, a method with minor change on the cabling design of the single current sensor is proposed in [27]. In [28], a fault detection, isolation and reconfiguration strategy against line current

Manuscript received January 28, 2019; revised April 21, 2019 and June 22, 2019; accepted August 10, 2019. This work was supported by Shaanxi Science Technology Co-ordination and Innovation Project, China (2013KTCQ01-20, 2016KTCQ01-49), Shaanxi Key Research and Development Program (2019GY-101) and Fundamental Research Funds for the Central Universities under Grants 3102019PB004.

J. Lu and J. Liu are with the School of Automation, Northwestern Polytechnical University (NWPU) and Shaanxi Key Laboratory of Small & Special Electrical Machine and Drive Technology of NWPU, Xi'an 710129, China. (E-mail: j.d.lu@nwpu.edu.cn, jinglinl@nwpu.edu.cn).

Y. Hu is with the Department of Electrical Engineering and Electronics, University of Liverpool, Liverpool L69 3GJ, U.K. (E-mail: y.hu35@liverpool.ac.uk) *(Corresponding author).*

Z. Wang is with the School of Electrical Engineering, Southeast University, Nanjing 210096, China. (E-mail: zwang@eee.hku.hk).

sensor failures is proposed, where a flux-linkage observer is used to estimate the current corresponding to the faulty phase.

However, in an IPMSM drive, none of the current sensors is guaranteed to be healthy, which means that the malfunctioning sensor can be either at the DC-bus side or phase side. Therefore, a security risk might exist in these strategies when the single survived current sensor does not happen to be located at the DC-bus side. If there is only one healthy phase current sensor, e.g., phase-A current sensor, neither the DC-bus current nor the other phase currents can be measured or reconstructed at any time or under any switching state.

The aforementioned security risk also exists in the IPMSM drive fed by a TPFS inverter. In [29], the current reconstruction strategy with a single DC-link current sensor in the TPFS inverter is proposed. However, as mentioned, if the phase-A current sensor alone survives (rather than the DC-bus current sensor), the reconstruction strategy will also become invalid. Moreover, as the DC-link current detected by the single sensor is actually the difference between two current values in [29], instead of the conventional DC-bus current, which means that re-cabling design of the single current sensor is needed for possible current reconstruction when the inverter topology alters from a three-phase six-switch (TPSS, conventional one) one to a TPFS one (reconfigured one).

Most of the strategies mentioned in the previous literatures aim at reconstructing the three-phase currents by using the single DC-bus current sensor. However, if one single phase current sensor survives, the above methods will become invalid. Additionally, in some methods that need minor changes on the current sensor cabling, the normal operation of the system will be greatly affected even if the current sensors are healthy [30]. Moreover, as the applied phase current sensors no longer detect the conventional three-phase currents, the three-phase currents cannot be correctly reconstructed during some periods. Therefore, the minimum action time for specific basic vectors is required for measuring the three-phase currents, resulting in the current measurement "dead zones" [31], [32]. Besides, most of these phase current reconstruction methods can only be applied to TPSS inverters. When the inverter is reconfigured to TPFS topology, these methods will also fail.

In order to deal with the aforementioned current reconstruction challenges with any of the survived current sensor, in this paper, an all current sensors survivable IPMSM drive is proposed. In the proposed drive, the current reconstruction strategy can be realized with any survived current sensor. Also, the proposed current reconstruction strategy can be applied in both the normal and reconfigured inverters without changing the proposed current sensor cabling. Most important of all, when all the current sensors are healthy, neither the normal operation of the drive nor the output voltage range of the inverter will be affected under no fault condition, except for the slight adjustments on the current sampling points in the high modulation areas (HMAs).

This paper is organized as follows. In Section II, the basic working principles of the proposed all current sensor survivable IPMSM drive are illustrated. In Sections III and IV, the current reconstruction methods under all current sensors survivable

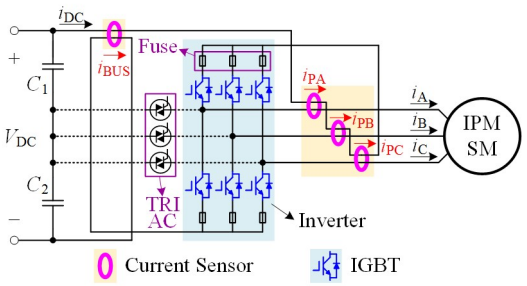

Fig. 1. The proposed all current sensors survivable IPMSM drive with reconfigurable inverter.

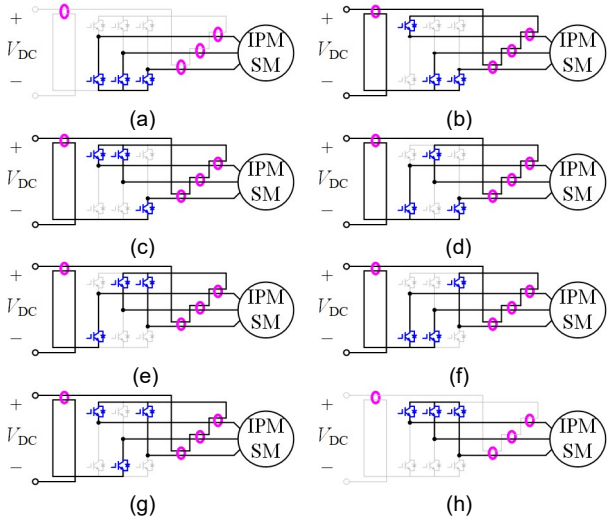

Fig. 2. Current paths under different switching states: (a) S_{000}, (b) S_{100}, (c) S_{110}, (d) S_{010}, (e) S_{011}, (f) S_{001}, (g) S_{101}, and (h) S_{111}.

situations in both the conventional and reconfigured inverter topologies are analyzed, respectively. In Section V, comparisons between the proposed and conventional strategies are illustrated. In Section VI, experimental results are presented. The conclusion is given finally in Section VII.

II. Proposed All Current Sensor Survivable IPMSM Drive with Reconfigurable Topology

The proposed all current sensors survivable IPMSM drive with reconfigurable inverter is presented in Fig. 1. In Fig. 1, i_{DC}, i_A, i_B, and i_C are DC-bus and three-phase currents; i_{BUS}, i_{PA}, i_{PB}, and i_{PC} are detected by the four current sensors. The triode alternating current semiconductor switches (TRIACs) and the quick fuses are utilized for inverter reconfiguration [33].

A. Sub-Circuits and Measured Currents in TPSS Inverter

When the drive is healthy, the current paths under different switching states, S_{000} - S_{111}, are presented in Fig. 2. It can be noticed that the four measured currents vary with the topology of sub-circuits. The relationships between the four current values and the switching states are presented in Table I. The DC-bus current is also given for comparison. It can be seen that i_{BUS} is always twice of i_{DC}. Therefore, when only the DC-bus current sensor survives, the proposed topology can also obtain the three-phase currents [16], [20].

It can be seen in both Fig. 2 and Table I that the three "phase-current-sensors" measure the actual three-phase

TABLE I
THE RELATIONSHIPS BETWEEN THE FOUR MEASURED CURRENTS AND THE SWITCHING STATES OF THE INVERTER.

Switching States (Action Vectors)	i_{BUS}	i_{DC}	i_{PA}	i_{PB}	i_{PC}
$S_{000}(V_0)$	0	0	i_A	i_B	i_C
$S_{100}(V_1)$	$2i_A$	i_A	$2i_A$	$-i_C$	$-i_B$
$S_{110}(V_2)$	$-2i_C$	$-i_C$	i_A-i_C	i_B-i_C	0
$S_{010}(V_3)$	$2i_B$	i_B	$-i_C$	$2i_B$	$-i_A$
$S_{011}(V_4)$	$-2i_A$	$-i_A$	0	$-i_A+i_B$	$-i_A+i_C$
$S_{001}(V_5)$	$2i_C$	i_C	$-i_B$	$-i_A$	$2i_C$
$S_{101}(V_6)$	$-2i_B$	$-i_B$	i_A-i_B	0	$-i_B+i_C$
$S_{111}(V_7)$	0	0	i_A	i_B	i_C

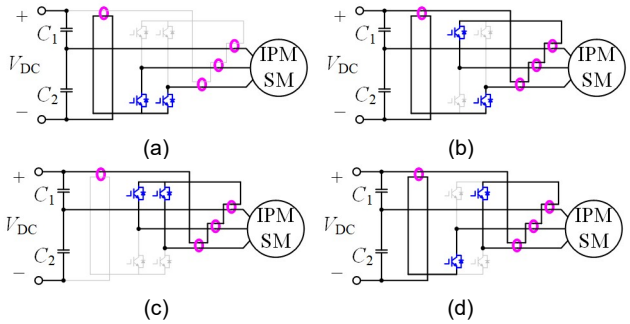

Fig. 3. Current paths with different switching states in reconfigured inverter topology: (a) S_{00}, (b) S_{10}, (c) S_{11}, and (d) S_{01}.

currents only under the switching states of S_{000} and S_{111}. Whereas during the other switching states, the measured currents no longer stand for the conventional ones.

B. Sub-Circuits and Measured Currents in TPFS Inverter

When one bridge arm open-circuit fault of the inverter encounters, e.g., phase-leg-A, the current paths in the reconfigured topology are presented in Fig. 3 with different switching states, S_{00} - S_{11}. It can be noticed that the relationships between the four current values and the switching states of the inverter are presented in Table II. It can be seen in both Fig. 3 and Table II that the three "phase-current-sensors" measure the actual three phase currents only under the switching state S_{00}. Whereas during the other switching states, the measured currents no longer stand for the conventional ones.

III. CURRENT SENSOR SURVIVABLE OPERATION PRINCIPLE IN TPSS TOPOLOGY

The sub-circuits of the proposed drive with TPSS topology are illustrated in Fig. 2. In the drive, there exists four current sensors. If some of these key sensors encounter faults, the normal current sampling process is affected. To solve this problem, current reconstruction strategies are applied. In this paper, the normal operation of the drive under the situations that only one current sensor survives is analyzed.

A. All Current Sensors Survived (Normal Operation)

If all the four current sensors survive, the normal operation of the proposed drive is very similar to that of the conventional "seven-segment SVPWM" strategy. Taking Section I for example, the PWM generating and current sampling strategies are illustrated in Fig. 4.

TABLE II
THE RELATIONSHIPS BETWEEN THE FOUR MEASURED CURRENTS AND THE SWITCHING STATES OF THE INVERTER.

Switching States	i_{BUS}	i_{PA}	i_{PB}	i_{PC}
S_{00}	i_A	i_A	i_B	i_C
S_{10}	i_B-i_C	$-i_C$	$2i_B$	$-i_A$
S_{11}	$-i_A$	0	$-i_A+i_B$	$-i_A+i_C$
S_{01}	$-i_B+i_C$	$-i_B$	$-i_A$	$2i_C$

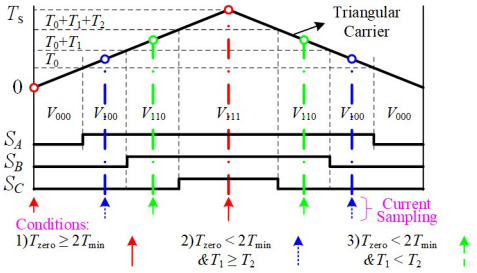

Fig. 4. The PWM generating and current sampling strategy in TPSS topology with all current sensors survived (Section I).

It can be seen from Fig. 4 that the PWM generation method has no difference with that of the "seven-segment SVPWM" one. In the figure, T_0, ..., T_7 represent the action time of the basic vectors V_0, ..., V_7, respectively. T_{zero} stands for the action time of zero vectors, which is the sum of T_0 and T_7. In order to ensure that the current measurement is not sampled near the switching action point, the minimum action time for basic vectors, T_{min}, within one PWM cycle, is required for accurate current sampling. T_{min} not only contains the switching device dead time but also the diode recovery time, AD sampling time and so on [27], [34]. Therefore, the current sampling methods vary with the action time of the basic vectors:

1) $T_{zero} \geq 2T_{min}$

In this case, both T_0 and T_7 are long enough for current sampling (no shorter than T_{min}). The two current sampling points are located at the beginning and middle of each PWM cycle. The measured currents i_{PA}, i_{PB}, and i_{PC} are equal to i_A, i_B, and i_C, respectively in both the two sampling points. Therefore, the actual three-phase currents are the average values of i_{PA}, i_{PB}, and i_{PC} measured at the two sampling points

$$\begin{cases} i_A = (i_{PA1}+i_{PA2})/2 \\ i_B = (i_{PB1}+i_{PB2})/2 \\ i_C = (i_{PC1}+i_{PC2})/2 \end{cases} \quad (1)$$

where i_{PA1}, i_{PB1}, i_{PC1} and i_{PA2}, i_{PB2}, i_{PC2} are the values of i_{PA}, i_{PB}, and i_{PC} measured at the two sampling points, respectively.

2) $T_{zero} < 2T_{min}$ & $T_1 \geq T_2$

However, if T_{zero} is not longer than $2T_{min}$, which means that neither T_0 nor T_7 is long enough for accurate current sampling, the output voltage vector locates in HMA. Therefore, either T_1 or T_2 must be long enough for accurate current sampling. Assuming that $T_1 \geq T_2$, the two current sampling points are located at the respective middle positions of the two action periods of V_1 in each PWM cycle. The measured currents are given in Table I, therefore, the actual three-phase currents can

TABLE III
THE ACTUAL THREE-PHASE CURRENT IN EACH SECTOR.

	Sector	i_A	i_B	i_C
I	$T_{zero} \geq 2T_{min}$	I_{PA}	I_{PB}	I_{PC}
	$T_{zero} < 2T_{min}$ & $T_1 \geq T_2$	$I_{PA} / 2$	$-I_{PC}$	$-I_{PB}$
	$T_{zero} < 2T_{min}$ & $T_1 < T_2$	$I_{PA} - I_{BUS} / 2$	$I_{PB} - I_{BUS} / 2$	$-I_{BUS} / 2$
II	$T_{zero} \geq 2T_{min}$	I_{PA}	I_{PB}	I_{PC}
	$T_{zero} < 2T_{min}$ & $T_2 \geq T_3$	$I_{PA} - I_{BUS} / 2$	$I_{PB} - I_{BUS} / 2$	$-I_{BUS} / 2$
	$T_{zero} < 2T_{min}$ & $T_2 < T_3$	$-I_{PC}$	$I_{PB} / 2$	$-I_{PA}$
III	$T_{zero} \geq 2T_{min}$	I_{PA}	I_{PB}	I_{PC}
	$T_{zero} < 2T_{min}$ & $T_3 \geq T_4$	$-I_{PC}$	$I_{PB} / 2$	$-I_{PA}$
	$T_{zero} < 2T_{min}$ & $T_3 < T_4$	$-I_{BUS} / 2$	$I_{PB} - I_{BUS} / 2$	$I_{PC} - I_{BUS} / 2$
IV	$T_{zero} \geq 2T_{min}$	I_{PA}	I_{PB}	I_{PC}
	$T_{zero} < 2T_{min}$ & $T_4 \geq T_5$	$-I_{BUS} / 2$	$I_{PB} - I_{BUS} / 2$	$I_{PC} - I_{BUS} / 2$
	$T_{zero} < 2T_{min}$ & $T_4 < T_5$	$-I_{PB}$	$-I_{PA}$	$I_{PC} / 2$
V	$T_{zero} \geq 2T_{min}$	I_{PA}	I_{PB}	I_{PC}
	$T_{zero} < 2T_{min}$ & $T_5 \geq T_6$	$-I_{PB}$	$-I_{PA}$	$I_{PC} / 2$
	$T_{zero} < 2T_{min}$ & $T_5 < T_6$	$I_{PA} - I_{BUS} / 2$	$-I_{BUS} / 2$	$I_{PC} - I_{BUS} / 2$
VI	$T_{zero} \geq 2T_{min}$	I_{PA}	I_{PB}	I_{PC}
	$T_{zero} < 2T_{min}$ & $T_6 \geq T_1$	$I_{PA} - I_{BUS} / 2$	$-I_{BUS} / 2$	$I_{PC} - I_{BUS} / 2$
	$T_{zero} < 2T_{min}$ & $T_6 < T_1$	$I_{PA} / 2$	$-I_{PC}$	$-I_{PB}$

be calculated by

$$\begin{cases} i_A = (i_{PA1} + i_{PA2})/4 \\ i_B = -(i_{PC1} + i_{PC2})/2 \\ i_C = -(i_{PB1} + i_{PB2})/2 \end{cases} \quad (2)$$

3) $T_{zero} < 2T_{min}$ & $T_1 < T_2$

Assuming that $T_1 < T_2$, the two current sampling points are located at the respective middle positions of the two action periods of V_2 in each PWM cycle. The measured currents are given in Table I, therefore, the actual three-phase currents are

$$\begin{cases} i_A = (i_{PA1} + i_{PA2})/2 - (i_{BUS1} + i_{BUS2})/4 \\ i_B = (i_{PB1} + i_{PB2})/2 - (i_{BUS1} + i_{BUS2})/4 \\ i_C = -(i_{BUS1} + i_{BUS2})/4 \end{cases} \quad (3)$$

where i_{BUS1} and i_{BUS2} are the values of i_{BUS} at the two sampling points, respectively.

In the other sectors, the PWM generation methods are also similar to that in sector I. Therefore, the actual three-phase currents in each sector can be calculated and are given in Table III. In the table, I_{BUS}, I_{PA}, I_{PB}, and I_{PC} are the average values of i_{BUS}, i_{PA}, i_{PB}, and i_{PC} measured at the two sampling points, respectively. The grey shading area indicates that the voltage vector is located in HMA.

It can be seen that the proposed strategy is very similar to that of the "seven-segment SVPWM" one, which does not affect the normal operation of the drive. Compared to the phase-leg-based fault-tolerant organization in [30], the output voltage range is not reduced due to the existence of T_{min}. Therefore, there is no limitation in the switching frequency for enlarging that region. Additionally, all the measured currents are not directly related to the inverter, therefore, the composition form of the inverter is not limited. Compared to those methods that require the measurements of the internal currents of the inverter [27], [30], the proposed scheme is more applicable.

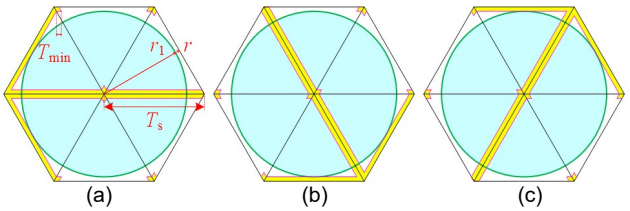

Fig. 5. The output voltage range when only one current sensor survived: (a) Phase-A, (b) Phase-B, and (c) Phase-C.

B. Single Current Sensor Survived (Phase-A)

If one single phase-current sensor survives, e.g., phase-A current sensor, only the current signal i_{PA} can be measured. In this case, it can be seen from Table I that the conventional "seven-segment SVPWM" strategy and corresponding current sampling methods are no longer applicable. Because under the switching state of S_{011} (action vector V_4), the measured current is zero. Whereas under the switching states of S_{000}, S_{100}, and S_{111} (action vectors V_0, V_1, and V_7), the measured currents are only related to i_A. It can be easily seen from Table I that the action time of the basic vectors should subject to the following rules to make the correct current reconstruction possible:

1) Sector I

$T_2 \geq T_{min}$; At least one of T_0 and T_1 is longer than T_{min}.

2) Sector II

At least two of T_0, T_2, and T_3 are longer than T_{min}.

3) Sector III

Both T_0 and T_3 are longer than T_{min}.

4) Sector IV

Both T_0 and T_5 are longer than T_{min}.

5) Sector V

At least two of T_0, T_5, and T_6 are longer than T_{min}.

6) Sector VI

$T_6 \geq T_{min}$; At least one of T_0 and T_1 is longer than T_{min}.

Limited by the above conditions, the output voltage range is presented in Fig. 5 (a). In Fig. 5 (a), the area surrounded by the pink line with yellow shading is the area that does not meet the above conditions. The area is also called the current reconstruction dead zones. In the "dead zone", the peripheral parts are within HMA of the output voltage, which cannot be eliminated by compensation. Therefore, the circular output voltage range is limited within the pale cyan shading area surrounded by green lines in case that the "dead zone" in this area are eliminated. The conditions that only phase-B or -C current sensor survives are illustrated in Fig. 5 (b) and (c).

The causes and compensation schemes of the "dead zone" within the circular output voltage range are:

1) Sector I

Causes: $T_2 < T_{min}$.

Compensation scheme: artificially increase T_2 to T_{min}, and using T_5 to compensate for the output vector.

Current sampling method: the first sampling point lies at the middle position of the bigger one between T_0 and T_1; the second sampling point lies at the middle position of T_2. The measured currents are i_A and $i_A - i_C$.

2) Sector II

Causes: $T_2 < T_{min}$ & $T_3 < T_{min}$.

Compensation scheme: increasing the longer one of T_2 and T_3 to T_{min}, and using T_5 (T_6) to compensate for the output vector.

Current sampling method: the first sampling point lies at the middle position of T_0; the second sampling point lies at the middle position of the longer one of T_2 and T_3. The measured currents are i_A and $i_A - i_C$ (or i_C).

3) Sector III

Causes: $T_3 < T_{min}$.

Compensation scheme: artificially increasing T_3 to T_{min}, and using T_6 to compensate for the output vector.

Current sampling method: the first sampling point lies at the middle position of T_0; the second sampling point lies at the middle position of T_3. The measured currents are i_A and i_C.

4) Sector IV

Causes: $T_5 < T_{min}$.

Compensation scheme: artificially increasing T_5 to T_{min}, and using T_2 to compensate for the output vector.

Current sampling method: the first sampling point lies at the middle position of T_0; the second sampling point lies at the middle position of T_5. The measured currents are i_A and i_B.

5) Sector V

Causes: $T_5 < T_{min}$ & $T_6 < T_{min}$.

Compensation scheme: increasing the longer one of T_5 and T_6 to T_{min}, and using T_2 (T_3) to compensate for the output vector.

Current sampling method: the first sampling point lies at the middle of T_0; the second one lies at the middle of the longer one of T_5 and T_6. The measured currents are i_A and i_B (or $i_A - i_B$).

6) Sector VI

Causes: $T_6 < T_{min}$.

Compensation scheme: artificially increasing T_6 to T_{min}, and using T_3 to compensate for the output vector.

Current sampling method: the first sampling point lies at the middle position of the bigger one of T_0 and T_1; the second sampling point lies at the middle position of T_6. The measured currents are i_A and $i_A - i_B$.

It should be noted that the PWM generation method only utilizes one of V_0 and V_7 for output voltage range enlargement in each PWM cycle. The current reconstruction strategies used when only phase-B or phase-C current sensor survives are similar to the case when phase-A current sensor survives.

IV. Current Sensor Survivable Operation Principle in TPFS Topology

The sub-circuits of the reconfigured drive are shown in Fig. 3. In this part, the normal operation of the drive along with the situations that only one current sensor survives are analyzed.

A. Single Current Sensor Survived (Faulty leg, Phase-A)

If the current sensor in the faulty leg, i.e., phase-A current sensor survives alone, only i_{PA} can be measured. It can be seen from Table II that no current information can be detected under switching state S_{11}, therefore, in this part the basic vectors V_{10} and V_{01} are utilized for zero vector synthesis. The PWM generation method applies three basic vectors in each PWM cycle, i.e., V_{10}, V_{00} (V_{11}), and V_{01}. For accurate current sampling, T_{10} and T_{01} are both artificially guaranteed to be longer than T_{min}. The measured currents are i_B and i_C. For better clarification, in this paper V_{DC1} and V_{DC2} represent the voltages on C_1 and C_2. The coordinate of the output voltage vector end point in α-β axis is denoted as P (x, y). The PWM generation and current sampling schemes can be refined to two parts:

1) $x \geq (V_{DC2} - V_{DC1}) / 2$

In this case, V_{10}, V_{00}, and V_{01} are utilized for PWM generating. The coordinates of P (x, y) should obey the following rules:

$$\begin{cases} x = (t_{00}/T_s)\cdot V_{DC2} + \left[(t_{10}+t_{01})/T_s\right]\cdot\left[(V_{DC2}-V_{DC1})/2\right] \\ y = \left[(t_{10}-t_{01})/T_s\right]\cdot\left[\sqrt{3}(V_{DC1}+V_{DC2})/2\right] \\ T_s = t_{00}+t_{10}+t_{01} \end{cases} \quad (4)$$

where t_{10}, t_{00}, t_{11}, and t_{01} are the action time of V_{10}, V_{00}, V_{11}, and V_{01} in this paper, respectively.

From (4), the action time of the basic vectors can be deduced:

$$\begin{cases} t_{00} = \left\{\left[2x-(V_{DC2}-V_{DC1})\right]/(V_{DC1}+V_{DC2})\right\}\cdot T_s \\ t_{10} = \left\{\left(-\sqrt{3}x+\sqrt{3}V_{DC2}+y\right)/\left[\sqrt{3}(V_{DC1}+V_{DC2})\right]\right\}\cdot T_s \\ t_{01} = \left\{\left(-\sqrt{3}x+\sqrt{3}V_{DC2}-y\right)/\sqrt{3}(V_{DC1}+V_{DC2})\right\}\cdot T_s \end{cases} \quad (5)$$

2) $x < (V_{DC2} - V_{DC1}) / 2$

In this case, V_{10}, V_{11}, and V_{01} are utilized for PWM generation. The coordinates of P (x, y) should obey the following rules:

$$\begin{cases} x = -(t_{11}/T_s)\cdot V_{DC1} + \left[(t_{10}+t_{01})/T_s\right]\cdot\left[(V_{DC2}-V_{DC1})/2\right] \\ y = \left[(t_{10}-t_{01})/T_s\right]\cdot\left[\sqrt{3}(V_{DC1}+V_{DC2})/2\right] \\ T_s = t_{11}+t_{10}+t_{01} \end{cases} \quad (6)$$

From (6), the action time of the basic vectors can be deduced:

$$\begin{cases} t_{11} = -\left\{\left[2x-(V_{DC2}-V_{DC1})\right]/(V_{DC1}+V_{DC2})\right\}\cdot T_s \\ t_{10} = \left\{\left(\sqrt{3}x+\sqrt{3}V_{DC1}+y\right)/\left[\sqrt{3}(V_{DC1}+V_{DC2})\right]\right\}\cdot T_s \\ t_{01} = \left\{\left(\sqrt{3}x+\sqrt{3}V_{DC1}-y\right)/\left[\sqrt{3}(V_{DC1}+V_{DC2})\right]\right\}\cdot T_s \end{cases} \quad (7)$$

Due to the artificially guaranteed minimum action time of T_{10} and T_{01}, the output voltage range will be limited to a certain area. Because the amplitudes of basic vectors V_{10} and V_{01} are much larger than those of V_{00} and V_{11}, the output voltage range are determined by the maximum voltages in the positive directions of V_{00} and V_{11} which are given below:

$$\begin{cases} \left|V_{max\_V00+}\right| = (V_{DC2}-V_{DC1})\cdot T_{min}/T_s + V_{DC2}\cdot(1-2T_{min}/T_s) \\ \left|V_{max\_V11+}\right| = (V_{DC1}-V_{DC2})\cdot T_{min}/T_s + V_{DC1}\cdot(1-2T_{min}/T_s) \end{cases} \quad (8)$$

Therefore, the limited circular output voltage range is:

$$\left|V_{\text{outmax}}\right| \le \sqrt{3}/2 \cdot \left[\min\left(V_{\text{DC1}}, V_{\text{DC2}}\right) - \left(V_{\text{DC1}} + V_{\text{DC2}}\right) \cdot T_{\min}/T_{\text{s}}\right] \quad (9)$$

B. Single Current Sensor Survived (Healthy leg, Phase-B)

If the healthy leg, e.g., phase-B current sensor survives alone, only i_{PB} can be measured. In this part the basic vectors V_{00} and V_{11} are utilized for zero vector synthesis. The PWM generation method applies three basic vectors in each PWM cycle, i.e., V_{00}, V_{10} (V_{01}), and V_{11}. For accurate current sampling, T_{00} and T_{11} are both artificially guaranteed to be longer than $T_{\min}$. The measured currents are i_{B} and $-i_{\text{A}} + i_{\text{B}}$ (Phase-B sensor) or i_{C} and $-i_{\text{A}} + i_{\text{C}}$ (Phase-C sensor). The PWM generating and current sampling schemes can be refined to two parts:

1) $y \ge 0$

In this case, V_{00}, V_{10}, and V_{11} are utilized for PWM generation. The coordinates of P (x, y) should obey the following rules:

$$\begin{cases} x = \left[t_{00} \cdot V_{\text{DC2}} - t_{11} \cdot V_{\text{DC1}} + t_{10} \cdot \left(V_{\text{DC2}} - V_{\text{DC1}}\right)/2\right]/T_{\text{s}} \\ y = \sqrt{3} t_{10} \cdot \left(V_{\text{DC1}} + V_{\text{DC2}}\right)/2T_{\text{s}} \\ t_{00} + t_{10} + t_{11} = T_{\text{s}} \end{cases} \quad (10)$$

From (10), the action time of the basic vectors are:

$$\begin{cases} t_{00} = \left\{\left(\sqrt{3}x - y + \sqrt{3}V_{\text{DC1}}\right)/\left[\sqrt{3}\left(V_{\text{DC1}} + V_{\text{DC2}}\right)\right]\right\} \cdot T_{\text{s}} \\ t_{11} = \left\{\left(-\sqrt{3}x - y + \sqrt{3}V_{\text{DC2}}\right)/\left[\sqrt{3}\left(V_{\text{DC1}} + V_{\text{DC2}}\right)\right]\right\} \cdot T_{\text{s}} \\ t_{10} = \left\{2y/\left[\sqrt{3}\left(V_{\text{DC1}} + V_{\text{DC2}}\right)\right]\right\} \cdot T_{\text{s}} \end{cases} \quad (11)$$

2) $y < 0$

In this case, V_{00}, V_{01}, and V_{11} are utilized for PWM generation. The coordinates of P (x, y) should obey the following rules:

$$\begin{cases} x = \left[t_{00} \cdot V_{\text{DC2}} - t_{11} \cdot V_{\text{DC1}} + t_{01} \cdot \left(V_{\text{DC2}} - V_{\text{DC1}}\right)/2\right]/T_{\text{s}} \\ y = -\sqrt{3} t_{01} \cdot \left(V_{\text{DC1}} + V_{\text{DC2}}\right)/2T_{\text{s}} \\ t_{00} + t_{01} + t_{11} = T_{\text{s}} \end{cases} \quad (12)$$

From (12), the action time of the basic vectors are:

$$\begin{cases} t_{00} = \left\{\left(\sqrt{3}x + y + \sqrt{3}V_{\text{DC1}}\right)/\left[\sqrt{3}\left(V_{\text{DC1}} + V_{\text{DC2}}\right)\right]\right\} \cdot T_{\text{s}} \\ t_{11} = \left\{\left(-\sqrt{3}x + y + \sqrt{3}V_{\text{DC2}}\right)/\left[\sqrt{3}\left(V_{\text{DC1}} + V_{\text{DC2}}\right)\right]\right\} \cdot T_{\text{s}} \\ t_{01} = -\left\{2y/\left[\sqrt{3}\left(V_{\text{DC1}} + V_{\text{DC2}}\right)\right]\right\} \cdot T_{\text{s}} \end{cases} \quad (13)$$

Similarly, due to the artificially guaranteed minimum action time of T_{00} and T_{11}, the output voltage range will be limited to a certain area. Also, the output voltage range are determined by the maximum voltages in the positive directions of V_{00} and V_{11}:

$$\begin{cases} \left|V_{\text{max\_V00+}}\right| = V_{\text{DC2}} - \left(V_{\text{DC1}} + V_{\text{DC2}}\right) \cdot \left(T_{\min}/T_{\text{s}}\right) \\ \left|V_{\text{max\_V11+}}\right| = V_{\text{DC1}} - \left(V_{\text{DC1}} + V_{\text{DC2}}\right) \cdot \left(T_{\min}/T_{\text{s}}\right) \end{cases} \quad (14)$$

Therefore, the limited circular output voltage range is:

$$\left|V_{\text{outmax}}\right| \le \sqrt{3}/2 \cdot \left[\min\left(V_{\text{DC1}}, V_{\text{DC2}}\right) - \left(V_{\text{DC1}} + V_{\text{DC2}}\right) \cdot T_{\min}/T_{\text{s}}\right] \quad (15)$$

It should be noted that the current reconstruction strategy when only phase-C current sensor survives is similar to that when phase-B sensor survives.

C. Other situations

1) All current sensors survive

In this case, it can be seen from Table II that under all switching states the four measured currents i_{BUS}, i_{PA}, i_{PB}, and i_{PC} are sufficient for three-phase current measurements. Therefore, the current sampling point should be placed at the middle point of the longest switching period of S_{00}, S_{10}, S_{11}, and S_{01}. The zero vector is synthesized by V_{00} and V_{11}. The PWM generation method is a symmetrical one: V_{00}, V_{10} (V_{01}), V_{11}, V_{10} (V_{01}), V_{00}.

2) Only the DC-bus current sensor survives

From Table II, it can be seen that the three-phase currents can be reconstructed during the action periods of any two adjacent basic vectors. It should be noted that all the output vectors can be synthesized by any two adjacent basic vectors [29].

D. Noise effect

It should be noted that the proposed current reconstruction strategy is based on the logical relationships among all the detected current values, i.e., i_{PA}, i_{PB}, i_{PC} and i_{BUS} according to different switching states (measuring actual motor currents on the same wire with different sensors). The measured currents for each current sensor only flow through the inverter before being injected into the motor windings, whereas other hardware devices such as the motor and other power devices are not included in the paths. Therefore, the relationships among all the detected currents are only determined by the topology and the switching status of the inverter as shown in Table I and Table II. Thus the influence of noise at the DC side on the proposed current reconstruction strategy itself can be neglected.

However, as shown in Fig.3, the fault phase winding is directly connected to the neutral point of the two DC-bus capacitors. Therefore, the deviations of the two capacitor voltages exist in the reconfigured inverter topology. This fluctuation in the DC-bus capacitor voltage affects the output voltage vector and cause motor current distortion. An effective compensation method used to balance the aforementioned two voltages is proposed in [35], which can be applied in the proposed all current sensor survivable IPMSM drive. Also, in order to minimize the impact of this voltage fluctuation on the output voltage vector, the capacitor voltage is sampled with a same frequency as control and PWM cycle frequency, which is 7.5 kHz in the experiment.

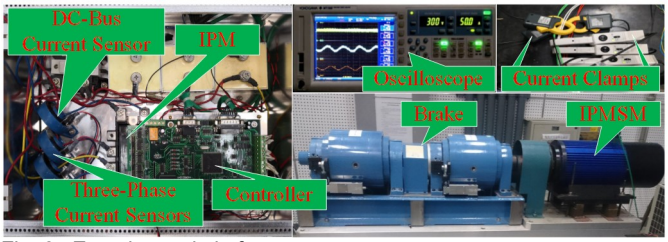

Fig. 6. Experimental platform.

V. Comparison to Conventional Strategies

The proposed all current sensors survivable IPMSM drive has many advantages compared to the conventional ones.

First, when the single survived current sensor is the DC-bus one, the proposed and conventional strategies do not show obvious differences [16], [20]. They all utilize the relationships between the DC-bus and three-phase current values for current reconstruction. However, no current sensor is guaranteed to be healthy, that is, if the single survived current sensor locates at the phase side, the proposed strategy can still work whereas the conventional ones do not. The reason is that in the conventional strategies, the phase current sensors detect the corresponding phase current values at any time and in any switching state.

Second, the proposed strategy does not need to measure the branch currents of the inverter and seldom affect the normal operation of the system when no fault is presented. In this paper, all the current measuring points for the proposed all current sensors survivable IPMSM drive are independent from the inverter, which means that the configuration of the inverter - integrated power module (IPM), three independent bridge arms or six power tubes - will not affect the proposed strategy. The current reconstruction strategies proposed in [18], [30] need to measure the branch currents within the inverter, which can only be applied in the inverters with six independent power tubes. In [27], the values of currents in the wrings that link the different bridge arms are measured for the proposed current reconstruction strategy - "zero voltage vector sampling method", which cannot be utilized in the IPM inverter.

At last, the proposed strategy realizes phase current reconstruction without changing the current sensors wirings after reconfiguration of the inverter, whereas the conventional strategy usually requires a re-cabling design of the current sensors. The cabling of the DC-bus current sensor in [29] for current reconstruction is the same as that in the conventional one [14] when the inverter does not encounter an open-circuit fault. However, if the inverter works in the fault-tolerant topology, the cabling of the DC-bus current sensor needs to be re-designed for its current reconstruction strategy.

VI. Experimental Validation

In order to verify the correctness of the proposed all current sensors survivable IPMSM drive, an experimental platform is set up as shown in Fig. 6. The main parameters of the IPMSM motor prototype used in the experiment are given in Table IV. The drive is supplied by a three-phase AC 380 V voltage source with a rectifier installed. The inverter applied in the drive is an intelligent power module, Mitsubishi PM75RLA120. The four current sensors, which are installed in the drive, are isolated hall-effect current sensors (HS01-100, maximum sample rate 100 kHz). In this paper, the measured currents for control (i_{ARE}, i_{BRE}, i_{CRE}) are all calculated in DSP by using the four hall-effect current sensors. Also, the three-phase and d-q axis current values and the estimated electromagnetic torque value are all sent to the host computer through RS-485. The actual three-phase currents (i_A, i_B, i_C, i_{DC}) and the detected currents (i_{PA}, i_{PB}, i_{PC}, i_{BUS}) are all re-detected by current clamps for comparison. The load is produced by the MAGTROL 30 kW dynamometer with a torque sensor installed. The main-control frequency, PWM cycle and voltage sampling frequency in the DC side are all set as 7.5 kHz.

TABLE IV
Main Parameters of IPMSM for Experiment.

Parameter	Value	Parameter	Value
Rated power	5 kW	Pole pairs	3
Inverter DC voltage	540 V	*d*-axis Inductance	4.2 mH
Rated voltage	380 V	*q*-axis Inductance	10.1 mH
Rated current	8.5 A	Phase resistance	0.18 Ω
Efficiency	0.9	Maximum speed	3000 r/min
Rated torque	15 N·m		

The conditions when the DC-bus current sensor survives alone have been reported in previous studies [16], [20], [29]. Therefore, these conditions are not included in the experiment.

A. Normal Operation of the Proposed Topology

When the proposed drive is healthy, the only difference between the conventional SVPWM strategy and the proposed one is the current sample method, especially for the method used between HMAs and low modulation areas (LMAs).

The waveforms of actual three-phase currents and the total harmonic distribution (THD) in HMAs and LMAs are displayed in Fig. 7. It can be seen that the waveforms of the actual currents are sinusoidal ones. The THDs are in the acceptable ranges under both HMAs and LMAs. In LMAs, the proposed topology and its control strategy has no difference from the normal one with SVPWM strategy.

The actual phase-A current i_A, the actual DC current i_{DC}, and the detected current i_{PA} in HMA are illustrated in Fig. 8. It can be seen that the detected current i_{PA} is the synthetic curve of i_A and i_{DC}. The same situation applies to i_{PB} and i_{PC}.

As displayed in Fig. 9, with the proposed current measurement strategy, the three-phase currents i_{ARE}, i_{BRE}, and i_{CRE} can be calculated from i_{PA}, i_{PB}, and i_{PC}. The calculated three-phase currents are in ladder-like waveforms, which are caused by the discrete current sampling. The THD of the calculated three-phase currents is about 5.47 %. It also can be seen that the calculated currents follow the actual ones even under the dynamic load-change conditions.

B. Fault-Tolerant Operation of the Proposed Strategy

If the proposed drive encounters an error, the fault-tolerant operation of the drive will be triggered. Because the situations that only the DC-bus current sensor survives in both the normal and reconfigured topologies have been studied in [20], [29], these cases will not be included in this Section.

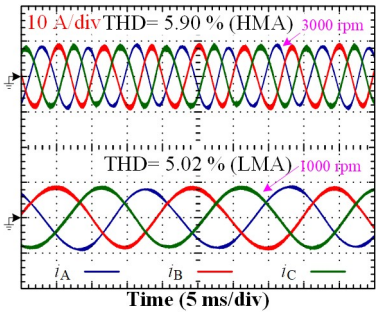

Fig. 7. Waveforms of actual three-phase currents and THD.

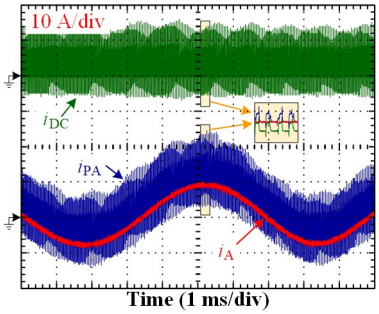

Fig. 8. The waveforms of i_A, i_{DC}, and i_{PA} in HMA.

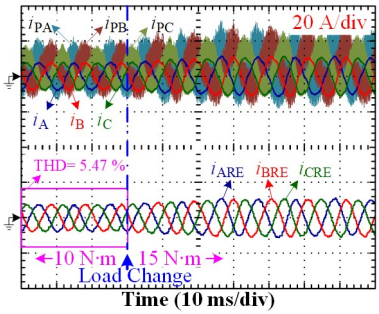

Fig. 9. Waveforms of actual and calculated three-phase currents during load change conditions in healthy condition.

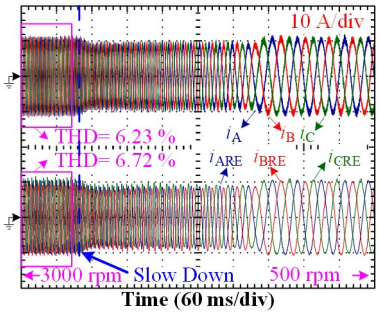

Fig. 10. Waveforms of actual and calculated three-phase currents during speed dynamic condition (Phase-A current sensor survives, TPSS).

When only the phase-A current sensor survives in TPSS inverter, as shown in Fig. 10, the actual and calculated three-phase currents under the speed dynamic condition are illustrated (speed changes from 3000 rpm to 500 rpm). It can be seen that during fast speed change condition, the reconstructed three-phase currents follow the actual ones accurately. Compared with Fig. 7, the THD of the actual three-phase currents is slightly increased, which is mainly caused by the asymmetric PWM generation strategy. Although the THD of the actual currents in Fig. 10 increases, the three-phase currents are still balanced. However, the calculated ladder-like currents show unbalanced curves, and the THD reaches 6.72 %. This is due to the use of asymmetrical PWM generation and asymmetrical current sampling strategy.

The experimental results of the actual and reconstructed currents when all the current sensors survive in the reconfigured topology during load sudden change are displayed in Fig. 11. The load changed suddenly from full load to 2 N·m. It can be seen that during this situation, the reconstructed three-phase currents follow the actual ones accurately.

In Fig.12, the actual and reconstructed d-q axis currents, i_d, i_q, i_{dre} and i_{qre}, are presented. It can be seen that the q-axis current decreases gradually from the beginning of the abrupt load change point. Whereas the d-axis current remains constant. The load torque T_L produced by the dynamometer and the estimated electromagnetic torque T_e are also given in Fig.12. It can be seen that as the load torque decreases, the electromagnetic torque also reduces.

The THD of the calculated ladder-like currents are smaller than that of the actual currents. This is due to the use of symmetrical PWM generating with symmetrical current sampling strategy. The current waveforms under the situation that only one phase current sensor survives in the reconfigured topology are similar to those when all the sensors survive. The THDs of the currents are displayed in Table V. It can be seen that the THDs of actual currents under different conditions are very close, which are all about 7 %. The THDs of the calculated currents with one single current sensor is slightly larger than that with all sensors survive. This is caused by the use of asymmetrical PWM generating strategy.

It can be seen from Table V, Fig. 10, and Fig. 11 that the worst working scenario for this proposed all current sensors survivable IPMSM drive is the situation when only single sensor survives. This is mainly due to the modified output voltage vector generation method and asymmetric current sampling strategy. This current sampling accuracy reduction and THD increment will cause degradation of system performance. However, this is a compromised scheme for fault situations, which enables the drive to have high fault-tolerant capability against current sensor failures.

In Fig.13, the waveforms of the obtained three-phase currents with phase current sensor failure are presented. In the figure, i_{A_PA}, i_{B_PB} and i_{C_PC} are the obtained three-phase currents with the installed phase current sensors; i_{A_DC}, i_{B_DC} and i_{C_DC} are the reconstructed three-phase currents using the installed DC-bus current sensor; i_{A_OBT}, i_{B_OBT} and i_{C_OBT} are the obtained three-phase currents for signal feed-back using the aforementioned current values. In Fig.13 (a), at the beginning, all the current sensors are in healthy conditions. At the middle, an artificial fault is added in the software, which results in the disappearance of the three-phase current sensor signals. After that, the fault-tolerant operation is triggered, and the single survived DC-bus current sensor is utilized to reconstruct the three-phase current values, so that the current feedback process is not interrupted by the faults in the phase-current sensors.

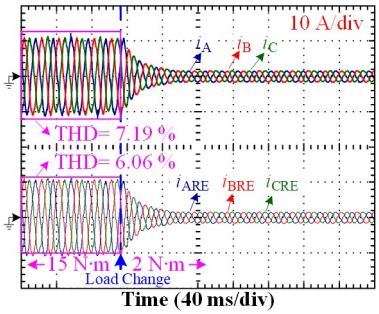

Fig. 11. Waveforms of actual and calculated three-phase currents during load change (All current sensors survive, reconfigured topology).

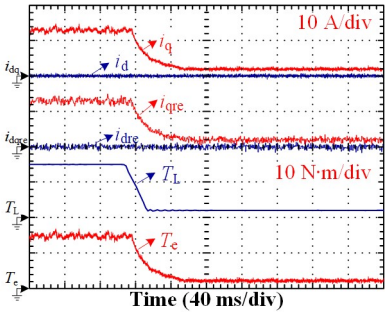

Fig. 12. Waveforms of actual and reconstructed d-q currents, load and estimated electromagnetic torque in Fig.11.

TABLE V
THDS OF ACTUAL AND CALCULATED CURRENTS.

Situation	THD	
	Actual Currents	Calculated Currents
All Sensors Survive	7.19 %	6.06 %
Fault-Phase Sensor Survives	6.71 %	6.28 %
Healthy-Phase Sensor Survives	7.03 %	6.14 %

In Fig.13 (b), the process of the fault-tolerant operation is illustrated. It can be seen that the obtained discrete three-phase current values are lost at the middle part of the waveform, which triggered the fault-tolerant operation. Then, after one PWM cycle, the current signals are reconstructed by using the single survived DC-bus current sensor. During the period of this fault-tolerant switching process, the feed-back current value will remain the same as that in the previous PWM cycle.

The waveforms of the obtained currents, α-β stator fluxes and motor torque are given in Fig.14. It can be seen that the stator currents in α-β axis are sinusoidal ones. During the fault-tolerant switching period of phase current sensor failure, which is at the middle of the waveform, the ladder-like current update is lost within one PWM cycle. However, it has little impact on the system performance. Besides, the stator flux remains in a circular shape. The torque ripple is relatively small, which is about ±0.5 N·m before the artificially introduced sensor fault. The torque fluctuation increases from the beginning of the fault-tolerant operation to about ±0.9 N·m, whereas the torque ripple is still within an acceptable range.

VII. CONCLUSION

Current sensors are essential components in motor drives. The previous current reconstruction strategies usually utilize

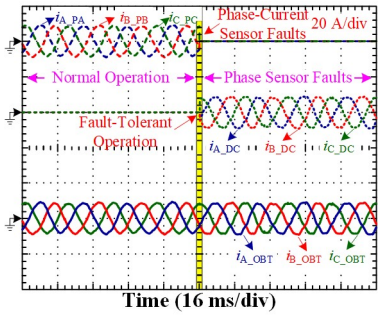

(a)

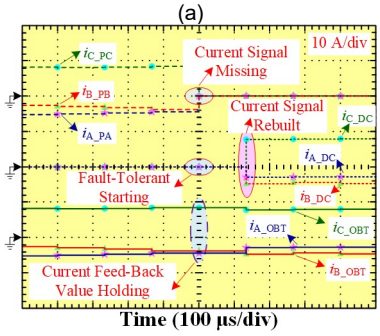

(b)

Fig. 13. Waveforms of obtained three-phase currents during phase current sensors failures: (a) Waveforms of the detected and obtained currents, (b) The process of fault-tolerant operation.

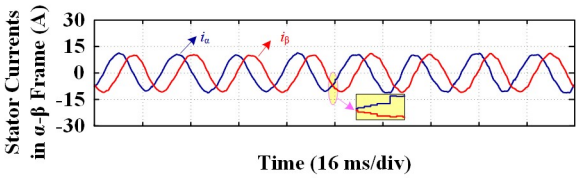

(a)

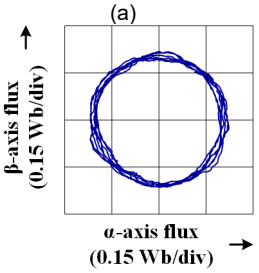

(b)

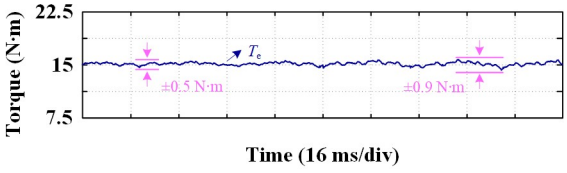

(c)

Fig. 14. Waveforms of obtained currents, stator flux and torque in Fig.13: (a) α-β axis currents, (b) Stator flux, (c) Torque.

the DC-bus current sensor to reproduce the three-phase currents. However, when the single survived current sensor is not the DC-bus current sensor, most of the strategies fail. Moreover, those schemes are applicable only in a certain inverter topology. In this paper, an all current sensors survivable IPMSM drive is proposed. The proposed fault-tolerant inverter topology can be utilized in the applications with high-reliability requirements, where the cost is not the main consideration, such as mine

ventilation, nuclear power station pump and so on.

1) The single survived current sensor can be either located at the DC-bus side or the phase side in the proposed topology for current reconstruction.
2) The cablings of the current sensors need no alteration when the topology of inverter changes.
3) The normal operation of the drive is not affected by the proposed reconfigurable inverter topology, and the output voltage range is also not reduced.
4) All the four measured currents are not related to the branch currents of the inverter, therefore, the proposed topology is more applicable.
5) The proposed all current sensors survivable IPMSM drive and the corresponding current reconstruction strategy is also applicable in drives with only two phase-current-sensors.
6) If the fault tolerance capability against inverter fault is not required, the additional hardware can be simply removed.

REFERENCES

[1] Z. Wang, Y. Zheng, Z. Zou, and M. Cheng, "Position sensorless control of interleaved CSI fed PMSM drive with extended Kalman filter," *IEEE Trans. on Magnetics,* vol. 48, no. 11, pp. 3688 - 3691, Nov. 2012.

[2] G. L. Wang, J. Y. Kuang, N. N. Zhao, G. Q. Zhang, and D. G. Xu, "Rotor position estimation of PMSM in low speed region and standstill using zero voltage vector injection," *IEEE Trans. Power Electron.,* vol. 33, no. 9, pp. 7948 - 7958, Sep. 2018.

[3] J. L. Liu, C. Gong, Z. X. Han, and H. Z. Yu, "IPMSM model predictive control in flux-weakening operation using an improved algorithm," *IEEE Trans. Ind. Electron.*, vol. 65, no. 12, pp. 9378-9387, Dec. 2018.

[4] F. F. Bu, H. Z. Liu, W. X. Huang, H. J. Xu, and Y. W. Hu, "Recent advances and developments in dual stator-winding induction generator and system," *IEEE Trans. Energy Converse.,* vol. 33, no. 3, pp. 1431-1442, Sep. 2018.

[5] W. Sun, Y. Yu, G. L. Wang, B. B. Li, and D. G. Xu, "Design method of adaptive full order observer with or without estimated flux error in speed estimation algorithm," *IEEE Trans. Power Electron.,* vol. 31, no. 3, pp. 2609-2626, Mar., 2016.

[6] C. Y. Wu, C. Q. Guo, Z. W. Xie, F. L. Ni, and H. Liu, "A signal-based fault detection and tolerance control method of current sensor for PMSM drive," *IEEE Trans. Ind. Electron.,* vol. 65, no. 12, pp. 9646-9657, Dec., 2018.

[7] B. Wang, X. L. Chen, Y. Yu, G. L. Wang, and D. G. Xu, "Robust predictive current control with online disturbance estimation for induction machine drives," *IEEE Trans. Power Electron.,* vol. 32, no. 6, pp. 4663-4674, June 2017.

[8] Y. H. Hu, C. Gan, W. P. Cao, J. F. Zhang, W. H. Li, and S. J. Finney, "Flexible fault-tolerant topology for switched reluctance motor drives," *IEEE Trans. Power Electron.,* vol. 31, no. 6, pp. 4654-4668, June, 2016.

[9] G. L. Wang, H. L. Zhou, N. N. Zhao, C. R. Li, and D. G. Xu, "Sensorless control of IPMSM drives using pseudo-random phase-switching fixed-frequency signal injection scheme," *IEEE Trans. Ind. Electron.,* vol. 65, no. 10, pp. 7660-7671, Oct. 2018.

[10] C. L. Xia, D. Wu, T. N. Shi, and W. Chen, "A current control scheme of brushless DC motors driven by four-switch three-phase inverters," *IEEE J. Em. Sel. Top. P.,* vol. 5, no. 1, pp. 547-558, Mar., 2017.

[11] B. E. Badsi, B. Bouzidi, and A. Masmoudi, "DTC Scheme for a Four-Switch Inverter-Fed Induction Motor Emulating the Six-Switch Inverter Operation," *IEEE Trans. Power Electron.,* vol. 28, no. 7, pp. 3528-3538, July, 2013.

[12] C. L. Xia, Z. Q. Li, and T. N. Shi, "A Control Strategy for Four-Switch Three-Phase Brushless DC Motor Using Single Current Sensor," *IEEE Trans. Ind. Electron.,* vol. 56, no. 6, pp. 2058-2066, June 2009.

[13] B. Metidji, N. Taib, L. Baghli, T. Rekioua, and S. Bacha, "Phase current reconstruction using a single current sensor of three-phase AC motors fed by SVM-controlled direct matrix converters," *IEEE Trans. Ind. Electron.,* vol. 60, no. 12, pp. 5497-5505, Dec. 2013.

[14] K. Him and T. M. Jahns, "Phase current reconstruction for AC motor drives using a DC link single current sensor and measurement voltage vectors," *IEEE Trans. Power Electron.,* vol. 21, no. 5, pp. 1413-1419, Sep. 2006.

[15] J. I. Ha, "Current prediction in vector-controlled PWM inverters using single DC-link current sensor," *IEEE Trans. Ind. Electron.,* vol. 57, no. 2, pp. 716-726, Feb. 2010.

[16] H. F. Lu, X. M. Cheng, W. L. Qu, S. Sheng, Y. T. Li, and Z. Y. Wang, "A three-phase current reconstruction technique using single DC current sensor based on TSPWM," *IEEE Trans. Power Electron.,* vol. 29, no. 3, pp. 1542-1550, Mar. 2014.

[17] G. L. Wang, R. Liu, N. N. Zhao, D. W. Ding, and D. G. Xu, "Enhanced linear ADRC strategy for HF pulse voltage signal injection-based sensorless IPMSM drives," *IEEE Trans. Power Electron.,* vol. 34, no. 1, pp. 514 - 525, Jan. 2019.

[18] Y. Cho, T. LaBella, and J. S. Lai, "A three-phase current reconstruction strategy with online current offset compensation using a single current sensor," *IEEE Trans. Ind. Electron.,* vol. 59, no. 7, pp. 2924-2933, Jul. 2012.

[19] K. Sun, Q. Wei, L. P. Huang, and K. Matsuse, "An overmodulation method for PWM-inverter-fed IPMSM drive with single current sensor," *IEEE Trans. Ind. Electron.,* vol. 57, no. 10, pp. 3395-3404, Oct. 2010.

[20] Y. K. Gu, F. L. Ni, D. P. Yang, and H. Liu, "Switching-state phase shift method for three-phase-current reconstruction with a single DC-link current sensor," *IEEE Trans. Ind. Electron.,* vol. 58, no. 11, pp. 5186-5194, Nov. 2011.

[21] H. Z. Ye and A. Emadi, "A six-phase current reconstruction scheme for dual traction inverters in hybrid electric vehicles with a single DC-link current sensor," *IEEE Transactions on Veh. Technol.,* vol. 63, no. 7, pp. 3085-3093, Sep. 2014.

[22] L. Jarzebowicz, "Errors of a linear current approximation in high-speed PMSM drives," *IEEE Trans. Power Electron.,* vol. 32, no. 11, pp. 8254-8257, Nov. 2017.

[23] F. R. Salmasi, "A self-healing induction motor drive with model free sensor tampering and sensor fault detection, isolation, and compensation," *IEEE Trans. Ind. Electron.*, vol. 64, no. 8, pp. 6105 - 6115, Aug. 2017.

[24] Y. Yu, Y. Z. Zhao, B. Wang, X. L. Huang, and D. G. Xu, "Current sensor fault diagnosis and tolerant control for VSI-based induction motor drives," *IEEE Trans. Power Electron.*, vol. 33, no. 5, pp. 4238 - 4248, May 2018.

[25] D. W. Chung and S. K. Sul, "Analysis and compensation of current measurement error in vector-controlled AC motor drives," *IEEE Trans. Ind. Appl.*, vol. 34, no. 2, pp. 340 - 345, Mar./Apr. 1998.

[26] M. Kim, S. K. Sul, and J. Lee, "Compensation of current measurement error for current-controlled PMSM drives," *IEEE Trans. Ind. Appl.*, vol. 50, no. 5, pp. 3365 - 3373, Sep./Oct. 2014.

[27] Y. X. Xu, H. Yan, J. B. Zou, B. C. Wang, and Y. H. Li, "Zero voltage vector sampling method for PMSM three-phase current reconstruction using single current sensor," *IEEE Trans. Power Electron.,* vol. 32, no. 5, pp. 3797-3807, May 2017.

[28] M. Manohar and S. Das, "Current sensor fault-tolerant control for direct torque control of induction motor drive using flux-linkage observer," *IEEE Trans. Ind. Informat.*, vol. 13, no. 6, pp. 2824 - 2833, Dec. 2017.

[29] J. D. Lu, Y. H. Hu, X. K. Zhang, Z. Wang, J. L. Liu, and C. Gan, "High frequency voltage injection sensorless control technique for IPMSMs fed by a three-phase four-switch inverter with a single current sensor," *IEEE/ASME Trans. Mechatronics*, vol. 23, no. 2, pp. 758-768, Apr. 2018.

[30] W. Jiang and B. Fahimi, "Current reconstruction techniques for survivable three-phase PWM converters," *IEEE Trans. Power Electron.,* vol. 25, no. 1, pp. 188-192, Jan. 2010.

[31] H. Yan, Y. X. Xu, J. B. Zou, Y. Fang, and F. Y. Cai, "A novel open-circuit fault diagnosis method for voltage source inverters with a single current sensor," *IEEE Trans. Power Electron.,* vol. 33, no. 10, pp. 8775-8786, Oct. 2018.

[32] X. Li, S. Dusmez, B. Akin, and K. Rajashekara, "A new SVPWM for the phase current reconstruction of three-phase three-level T-type converters," *IEEE Trans. Power Electron.,* vol. 31, no. 3, pp. 2627-2637, Mar. 2016.

[33] Y. W. Hu, L. H. Zhang, W. X. Huang, and F. F. Bu, "A fault-tolerant induction generator system based on instantaneous torque control (ITC)," *IEEE Trans. Energy Converse.,* vol. 25, no. 2, pp. 412-421, June 2010.

[34] Z. Y. Zhang, H. F. Lu, D. J. Costinett, F. Wang, L. M. Tolbert, and B. J. Blalock, "Model-based dead time optimization for voltage-source converters utilizing silicon carbide semiconductors," *IEEE Trans. Power Electron.,* vol. 32, no. 11, pp. 8833-8844, Nov. 2017.

[35] Z. Y. Zeng, W. Y. Zheng, R. X. Zhao, C. Zhu, and Q. W. Yuan, "Modeling, modulation and control of the three-phase four-switch PWM rectifier under balanced voltage," *IEEE Trans. Power Electron.*, vol. 31, no. 7, pp. 4892-4906, July, 2016.

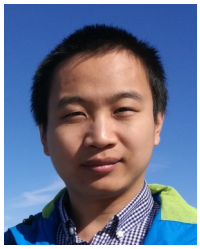

Jiadong Lu (M'19) was born in Pucheng, China, 1990. He received the B.S., the M.S. and the Ph.D. degrees in electrical engineering from Northwestern Polytechnical University (NWPU), Xi'an, China in 2012, 2015 and 2018, respectively. Between 2017 and 2018, he was with the Department of Electrical Engineering, Electronics and Computer Science, University of Liverpool (UoL), U.K. as an Honorary Academic Researcher. Currently, he is an Associate Research Fellow at the Department of Electrical Engineering, NWPU.

His research interests include hybrid-fault-tolerant control techniques for permanent magnet synchronous motor drives, aging issue for motor drives and power electronics converters & control.

Yihua Hu (M'13-SM'15) received the B.S. degree in electrical engineering in 2003, and the Ph.D. degree in power electronics and drives in 2011, both at China University of Mining and Technology. Between 2011 and 2013, he was with the College of Electrical Engineering, Zhejiang University as a Postdoctoral Fellow. Between 2013 and 2015, he worked as a Research Associate at the power electronics and motor drive group, the University of Strathclyde. Between 2016 and 2019, he was a Lecturer at the Department of Electrical Engineering and Electronics, University of Liverpool (UoL). Currently, he is a reader at Electronics Engineering Department at University of York (UoY). He has published 85 papers in IEEE Transactions journals. His research interests include renewable generation, power electronics converters & control, electric vehicle, more electric ship/aircraft, smart energy system and non-destructive test technology. He is the associate editor of IEEE Transactions on Industrial Electronics, IET Renewable Power Generation, IET Intelligent Transport Systems and Power Electronics and Drives.

Zheng Wang (S'05–M'09-SM'14) received the B.Eng. and M.Eng. degrees from Southeast University, Nanjing, China, in 2000 and 2003, respectively, and the Ph.D. degree from The University of Hong Kong, Hong Kong, in 2008, all in electrical engineering.

From 2008 to 2009, he was a Postdoctoral Fellow in Ryerson University, Toronto, ON, Canada. He is currently a full Professor in the School of Electrical Engineering, Southeast University, China. His research interests include electric drives, power electronics, and distributed generation. He has authored or coauthored over 80 internationally refereed papers and four books in these areas.

Prof. Wang received several academic awards including IEEE PES Chapter Outstanding Engineer Award, Best Paper Award of ICMES, Best Session Paper Award of IECON, and Nanjing Outstanding Paper Award of Natural Science.

Jinglin Liu (M'01) received the B.Eng. degree in electrical engineering from Tsinghua University, Beijing, China, in 1986, and the M.Eng. and the Ph.D. degrees in electrical engineering from NWPU, Xi'an, China, in 1990 and 2002, respectively. Since 1994, he has been a Faculty Member with NWPU, Xi'an, where he is currently a Professor of Electrical Engineering. His research interests include electrical machines design and drives, power electronics, fault diagnosis, and motion control.